



## Biomaterials Science

### Supporting Information

#### Electronic Supplemental Information

*for*

#### **Universal Nanothin Silk Coatings via Controlled Spidroin Self-Assembly**

R. Helen Zha,<sup>\*a</sup> Peyman Delparastan,<sup>b</sup> Tanner D. Fink,<sup>a</sup> Joschka Bauer,<sup>c</sup> Thomas Scheibel,<sup>c</sup> Phillip B. Messersmith<sup>b</sup>

*\*corresponding author*

*a. Department of Chemical & Biological Engineering, Rensselaer Polytechnic Institute, 110 8th St., Troy, NY, 12180.*

*b. Department of Materials Science and Engineering, Department of Bioengineering, University of California – Berkeley, Berkeley, CA 94720.*

*c. Department for Biomaterials, University of Bayreuth, 95440 Bayreuth, Germany.*

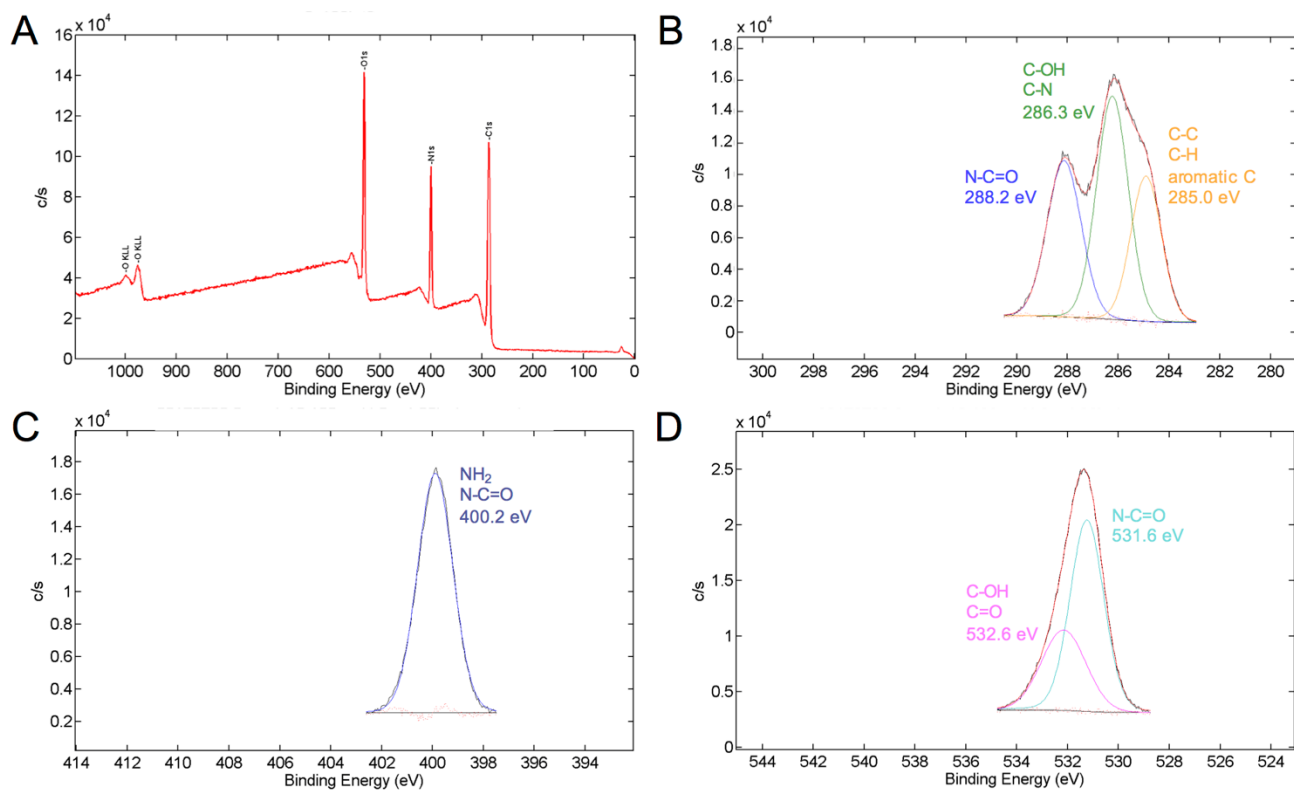


**Figure S1.** A) XPS spectrum of TiO<sub>2</sub> samples coated by immersion for 30 hrs in 2 mg/mL eADF4(C16) with 100 mM KH<sub>2</sub>PO<sub>4</sub> (25 mM bicine buffer, pH 8.5, 100 mM NaCl). N1s, O1s, O KLL, and C1s signals are visible in this survey scan. High resolution scans of the B) C1s region, C) N1s region, and D) O1s region. Deconvolution fits are shown with peak locations listed in corresponding colors.

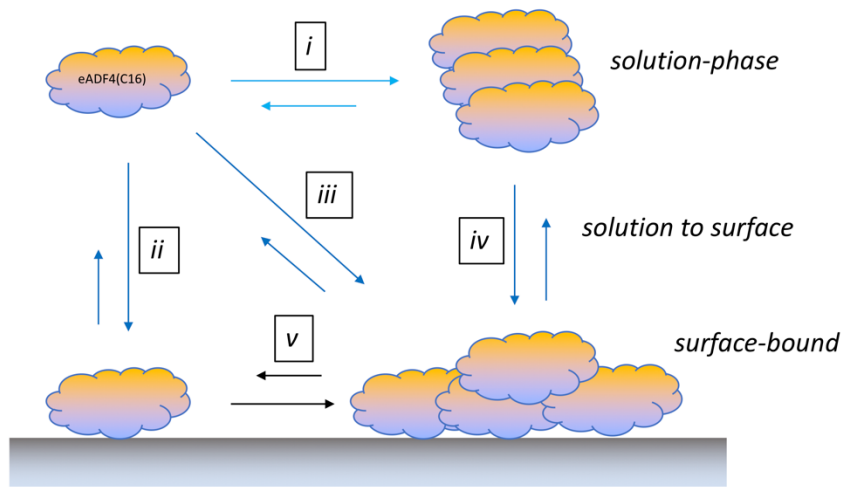


**Figure S2.** Proposed underlying mechanisms of spidroin coating self-assembly, including i) solution-phase protein assembly, ii) non-specific adsorption of protein monomers to the surface, iii) assembly of protein monomers with existing protein aggregates on the surface, iv) non-specific adsorption of protein aggregates to the surface, and v) conformation change and/or aggregation of surface-bound proteins. The interplay of these mechanisms likely depends on surface energy, solution conditions, and protein sequence.

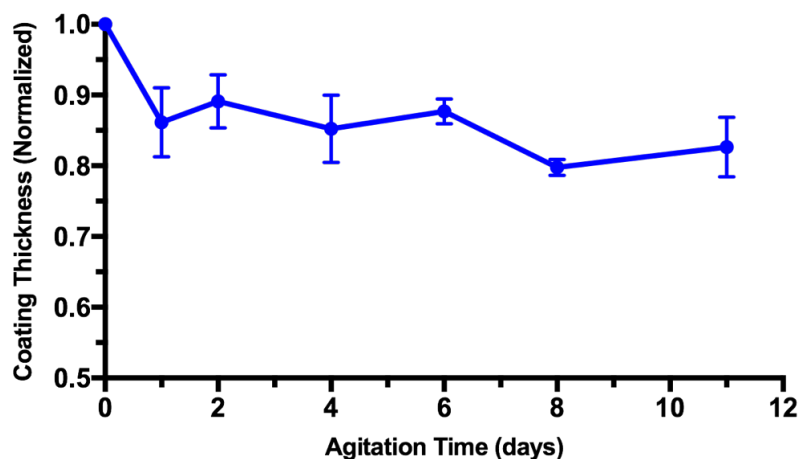


**Figure S3.** Change in eADF4(C16) coating thickness after prolonged agitation in HEPES buffer (pH 7.4, 150 mM NaCl, 37 °C) as measured by ellipsometry. Coatings were made by immersing TiO<sub>2</sub> substrates in 0.5 mg/mL eADF4(C16) with 200 mM KH<sub>2</sub>PO<sub>4</sub> in 25 mM bicine buffer (pH 8.5, 100 mM NaCl, room temperature) for 20 hrs, yielding coatings initially 21.3 ± 0.7 nm thick in the dry state at day 0. Coated substrates were agitated at 60 RPM in an incubated orbital shaker. After 1, 2, 4, 6, 8, or 11 days, samples were removed, gently rinsed, and dried for measurement by ellipsometry. For each sample, the coating thickness was normalized to its initial thickness, and the average normalized thickness at each time point is shown (n = 3).

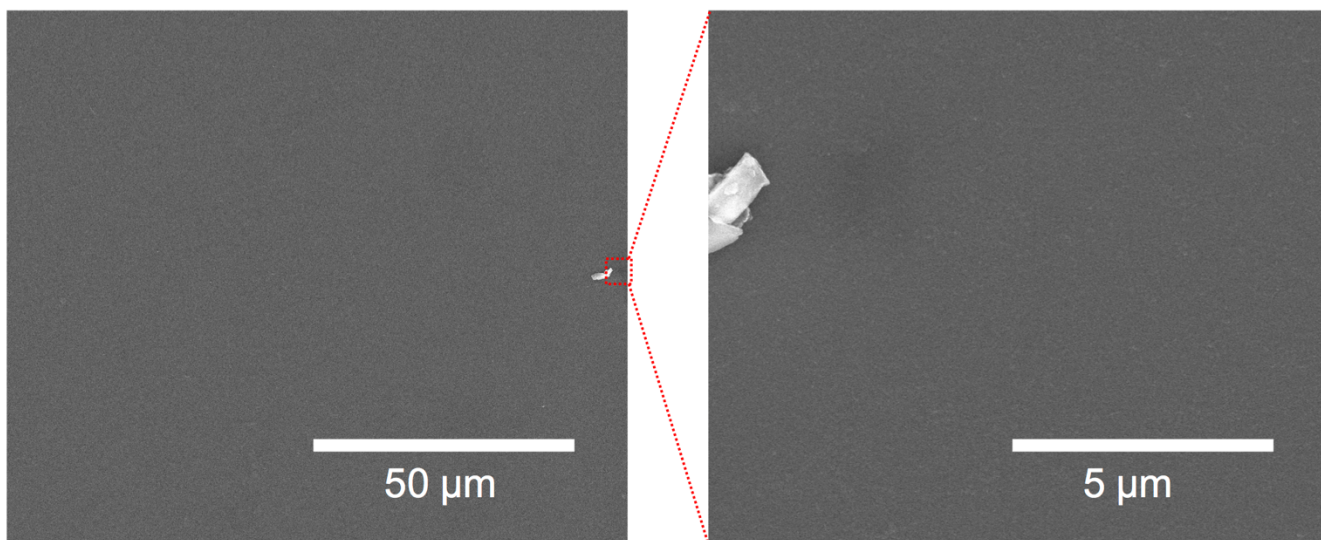
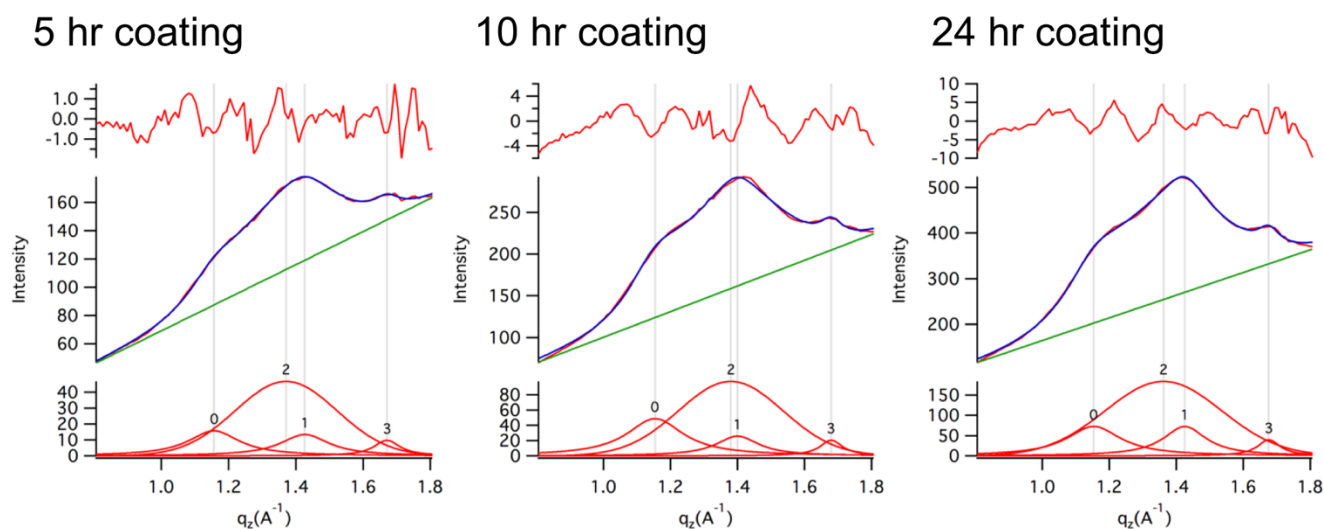


**Figure S4.** SEM image of  $\text{TiO}_2$  substrates coated by immersion for 30 hrs in 2 mg/mL eADF4(C16) with 100 mM  $\text{KH}_2\text{PO}_4$  (25 mM bicine buffer, pH 8.5, 100 mM NaCl). A low magnification (1250X) image is shown on the left and a high magnification (12500X) image is shown on the right. One dust particle is included in the image for context.



Coating time	(200)	(120)	(121)	amorphous halo	% crystallinity
5 hr	0.179	0.142	0.041	0.638	35.4
10 hr	0.250	0.101	0.042	0.607	39.3
24 hr	0.166	0.135	0.053	0.646	36.2

**Figure S5.** 1D radial reductions of 2D GIWAXS scattering images in the range of  $0.8 \text{ \AA}^{-1} < |q| < 1.8 \text{ \AA}^{-1}$  for eADF4(C16) coatings on silicon wafer made with 5 hrs, 10 hrs, and 24 hrs coating time. Deconvoluted peaks are shown in the bottom panels, where 0 corresponds to the (200) reflection, 1 corresponds to the (120) reflection, 2 corresponds to the amorphous halo, and 3 corresponds to the (121) reflection. Radial reductions (red) and the summation of deconvoluted peaks (blue) are shown in the middle panels. Residual fit errors are shown in the top panels. Normalized peak areas and % crystallinity for each coating are listed in the table.

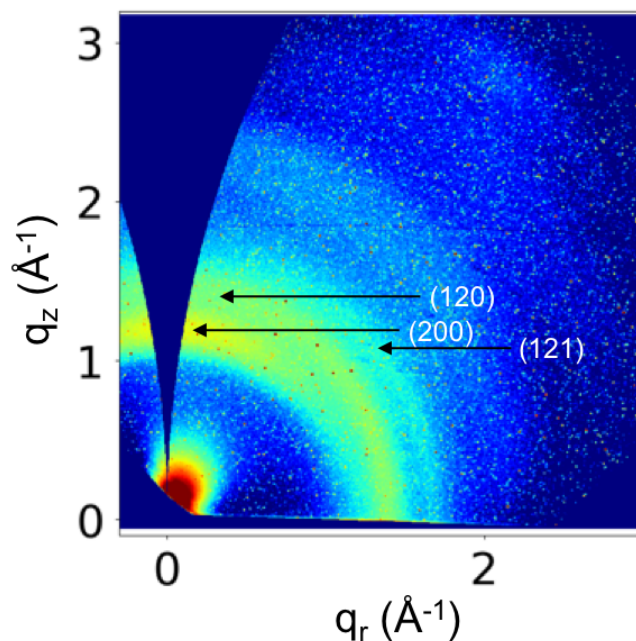


**Figure S6.** 2D GIWAXS detector image of eADF4(C16) self-assembled on TiO<sub>2</sub> substrate (100 nm TiO<sub>2</sub> deposited on silicon wafer with 2 nm native oxide). Coatings were fabricated by immersing cleaned substrates in 0.5 mg/mL eADF4(C16) with 200 mM KH<sub>2</sub>PO<sub>4</sub> and 100 mM NaCl in 10 mM bicine buffer for 24 hrs as described in the Experimental section of the main text. The CMS beamline (11-BM) at the National Synchrotron Light Source II (Brookhaven National Lab) was used to acquire this data, and the raw detector image has been converted to ( $q_r$ ,  $q_z$ ) space. The expected  $|q|$  of the (200), (120), and (121) Bragg reflections are indicated. Anisotropic scattering with increased intensity along the  $q_z$  axis is noticeable, particularly for the (200) reflection, suggesting orientation of the  $\beta$ -sheets. Though these results on TiO<sub>2</sub> are similar to results found on Si, quantitative analysis was performed using self-assembled eADF4(C16) coatings on silicon due to the higher noise and lower scattering intensity seen here.

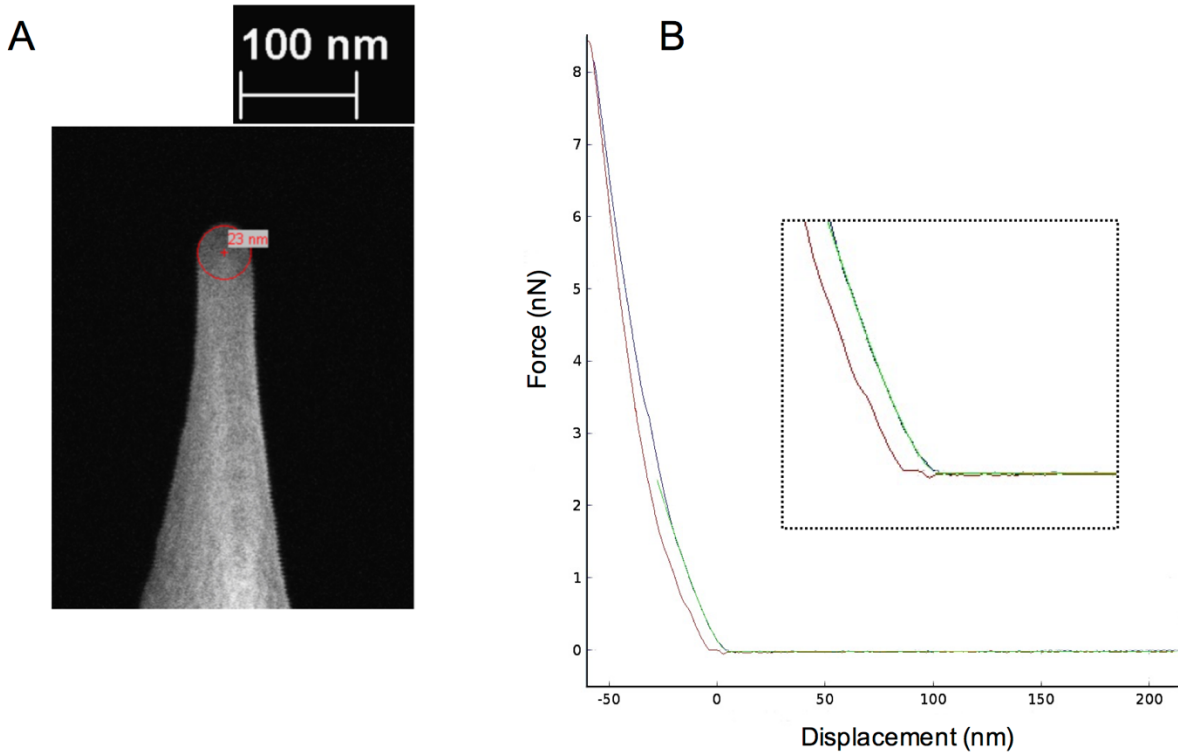


**Figure S7.** A) SEM image of AFM tip with a spherical nanoindenter 23 nm in diameter. B) A representative force-distance curve obtained in nanoindentation experiments. The approach curve is shown in blue and the retraction curve is shown in purple. The elastic region of the approach curve (inset) is fitted with Hertz model (fit shown in green) and Young's modulus is extracted using the following equation for spherical indenters:

$$F = \frac{4}{3} \left[ \frac{E}{(1 - \nu^2)} \right] \delta^{3/2} \sqrt{R}$$

where  $F$  is the force applied,  $\delta$  is the indentation depth,  $R$  is the indenter radius,  $E$  is the Young's modulus of the indented material, and  $\nu$  is the Poisson's ratio of the indented material (assumed to be 0.5).

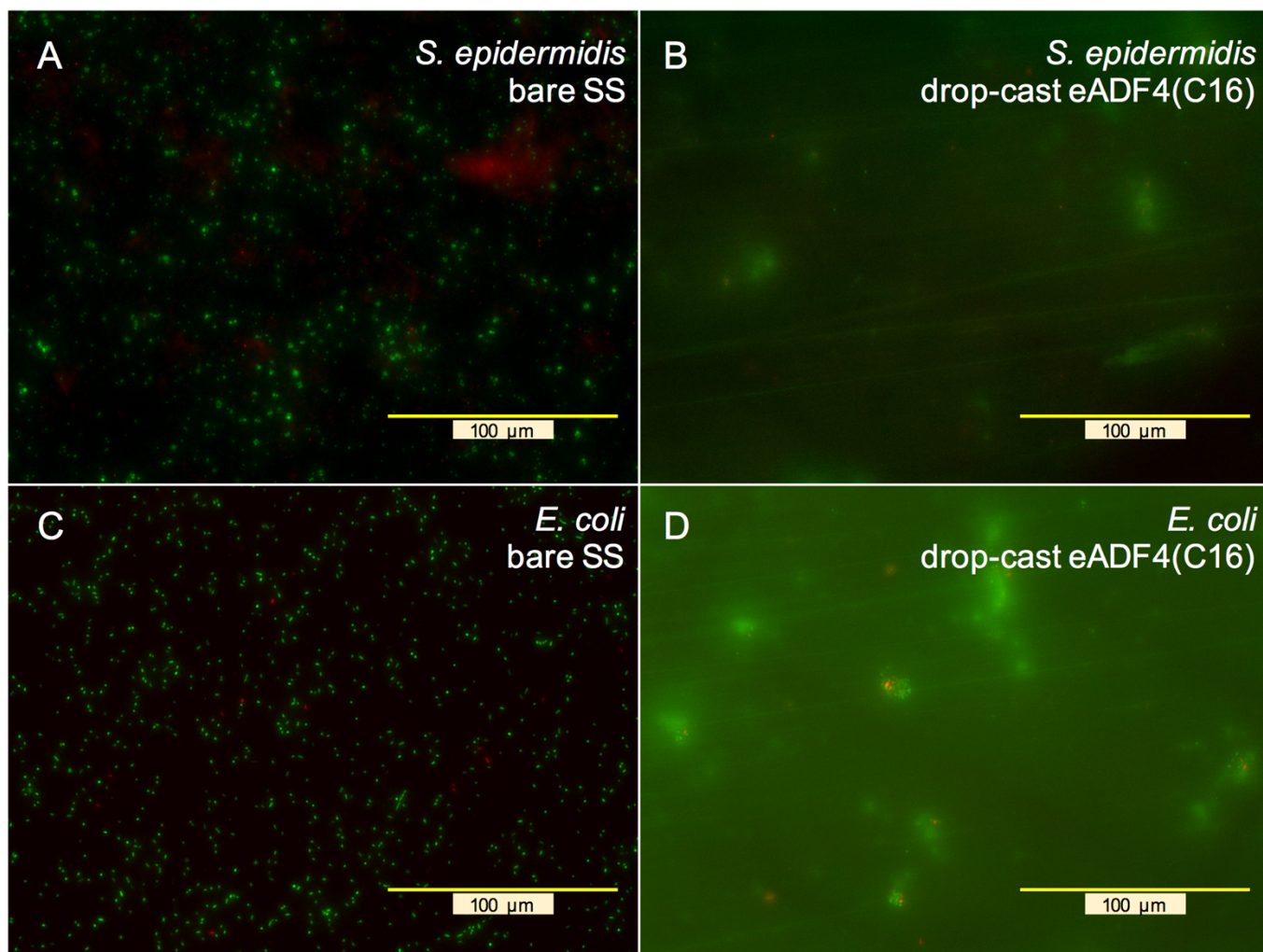


**Figure S8.** Representative fluorescence microscopy of *S. epidermidis* (A-B) and *E. coli* (C-D) adhered to bare stainless steel and stainless steel with a layer of eADF4(C16) fabricated by drop-casting from HFIP with methanol post-treatment. Propidium iodide was used to stain for dead cells (red) and SYTO 9 was used for live cells (green). Diffuse background staining of the eADF4(C16) coating is visible due to the thickness of the drop-cast layer.